Magnesium Technology 2011
Edited by: Wim H. Sillekens, Sean R. Agnew, Neale R. Neelameggham, and Suveen N. Mathaudhu
TMS (The Minerals, Metals & Materials Society), 2011

ON PREDICTING THE CHANNEL DIE COMPRESSION BEHAVIOR OF HCP MAGNESIUM AM30 USING CRYSTAL PLASTICITY FEM

Q. Ma[1], E.B. Marin[1], A. Antonyraj[1], Y. Hammi[1], H. El Kadiri[1,2], P.T. Wang[1], M.F. Horstemeyer[1,2]
[1] Center for Advanced Vehicular Systems, Mississippi State University, Mississippi State, MS 39762, USA
[2] Department of Mechanical Engineering, Mississippi State University, Mississippi State, MS 39762, USA

Keywords: Magnesium, Texture, Plasticity, 3D microstructure, Modeling

Abstract

Deformation of polycrystalline aggregates of HCP crystals was investigated by employing crystal plasticity and finite element simulations. Results were validated using channel die compression tests. The three dimensional polycrystal, represented by Voronoi techniques, was assigned an initial distribution of crystallographic orientations determined from X-Ray Diffraction. The mechanical properties from the channel die compression tests were used to correlate the material parameters of the crystal plasticity model. Simulations predicted grain-to-grain interactions and the resulting texture evolution under channel die compression. The inhomogeneous deformation among grains was mapped by a stress and a strain distribution and grain orientation spread. The simulation results were compared with experimental observations of an HCP polycrystal subjected to channel die compression.

Introduction

Plastic straining of a polycrystal induces changes in the crystals orientation and the corresponding evolution of orientation distributions oftentimes called crystallographic texture. Texture governs the anisotropic mechanical properties of a polycrystal, e.g. yield surface and strain ratio (Lankford parameter) [1,2]. As texture evolution is intrinsically tied to the activation of slip systems and twinning systems, a number of deformation models incorporating texture, slip, and twinning have been developed in the last decades [3-12]. Two pioneering deformation models for polycrystals are the upper-bound and lower-bound theories, typically referred to as Taylor and Sachs models [3-4]. These models considered only strain compatibility and stress equilibrium, respectively, hence simplifying intricate interactions among grains within a polycrystal which resulted in a marked discrepancy between predicted and experimental textures [5]. Other models, called relaxed constraint models, are modifications of Taylor and Sachs models. For example, modified Taylor models [6,7] relaxed partly the strain compatibility condition; a modified Sachs model [8] considered reaction shear stresses between local grains and its neighborhood represented by the whole matrix; the Visco-Plastic Self-consistent (VPSC) model [9] satisfied the stress and strain equilibrium simultaneously by considering individual grains embedded in an effective medium, whose property was represented by the average of the polycrystalline aggregate. These modified models improved the texture prediction; however, most of these models did not consider the topological information of grains [5-12].

The crystal plasticity finite element model (CPFEM) combined the single crystal plasticity constitutive law with finite elements to compute the macroscale response of crystal aggregates [10,11]. In CPFEM, the equilibrium of forces (stresses) and the compatibility of displacements are implicitly satisfied by the finite element formulation. This technique can be used to model two dimensional (2D) or three dimensional (3D) microstructures [10-15] to investigate many aspects of the heterogeneous plastic response of a local grain within a polycrystal under various boundary conditions [14]. At present, 3D CPFEM deformation simulations attract more attention as 3D microstructure deformation resembles the realistic deformation of polycrystals. In this context, the use of a fine meshed regular polyhedron representing a grain with a particular orientation has been widely used to investigate intragranular orientation gradient and grain interaction effects during deformation. Many CPFEM studies have used brick-shape grains [16], rhombic dodecahedron grains [13,14,17], and tetradecahedron grains [15] to investigate grain interaction effects on texture evolution, grain subdivision and strain localization. However, as suggested by Mika and Dawson [18,19], crystal shape could also play a large role on texture scatter, and hence, the use of uniform and regular grain shapes can still produce a discrepancy between experimental textures and simulations.

This article investigates the plane strain deformation of a polycrystal aggregate using the CPFEM and 3D Voronoi grains. The focus is on revealing the effect of grain interaction on global texture evolution, intergranular heterogeneous plasticity, and intragranular orientation spread. The material studied is HCP AM30 magnesium alloy.

Crystal Plasticity Constitutive Framework

The constitutive framework adopted in this paper corresponds to the formulation presented in [20,21]. This formulation is an extension of a rigid viscoplastic model to account for elasticity effects, and incorporates a number of changes with respect to a previous formulation [22]. The model can be summarized as follows:

$$\mathbf{d} = \overset{\nabla}{\boldsymbol{\epsilon}}^e + \tilde{\mathbf{D}}^p, \quad \overset{\nabla}{\boldsymbol{\epsilon}}^e = \dot{\boldsymbol{\epsilon}}^e + \boldsymbol{\epsilon}^e\tilde{\Omega}^e - \tilde{\Omega}^e\boldsymbol{\epsilon}^e \tag{1}$$

$$\mathbf{w} = -skew(\dot{\boldsymbol{\epsilon}}^e\boldsymbol{\epsilon}^e) + \tilde{\Omega}^e + \tilde{\mathbf{W}}^p, \quad \tilde{\Omega}^e = \dot{\mathbf{R}}^e\mathbf{R}^{eT} \tag{2}$$

$$\tau = \tilde{\mathbb{C}}^e : \boldsymbol{\epsilon}^e \tag{3}$$

$$\tilde{\mathbf{D}}^p = \sum_{\alpha=1}^{N} \dot{\gamma}^\alpha sym(\tilde{\mathbf{S}}^\alpha \otimes \tilde{\mathbf{m}}^\alpha) \tag{4}$$

$$\tilde{\mathbf{W}}^p = \sum_{\alpha=1}^{N} \dot{\gamma}^\alpha skew(\tilde{\mathbf{S}}^\alpha \otimes \tilde{\mathbf{m}}^\alpha) \tag{5}$$

$$\dot{\gamma}^\alpha = \dot{\gamma}_0 \left(\frac{|\tau^\alpha|}{\kappa^\alpha} \right)^{1/m} sign(\tau^\alpha) \tag{6}$$

$$\tau^{\alpha} = \tau : sym(\tilde{\mathbf{S}}^{\alpha} \otimes \tilde{\mathbf{m}}^{\alpha}) \tag{7}$$

$$\dot{\kappa}^{\alpha} = h_0 \left(\frac{\kappa_S - \kappa}{\kappa_S - \kappa_0} \right) \sum_{\alpha} \left| \dot{\gamma}^{\alpha} \right| \tag{8}$$

Where $\boldsymbol{d}$ is the deformation rate, $\overset{\nabla}{\epsilon}^{e}$ is the elastic deformation rate, $\tilde{\mathbf{D}}^{p}$ is the plastic deformation rate, $\boldsymbol{w}$ is the spin tensor and ϵ^{e} is the small elastic tensor. $\tilde{\Omega}^{e}$ is the elastic lattice spin tensor, $\tilde{\mathbf{W}}^{p}$ is the plastic spin tensor, $\mathbf{R}^{e}$ is the lattice rotation tensor, τ is the stress tensor, $\tilde{\mathbb{C}}^{e}$ is the fourth order anisotropic crystal elasticity tensor and $\tilde{\mathbf{S}}^{\alpha} \otimes \tilde{\mathbf{m}}^{\alpha}$ defines the Schmid tensor. $\dot{\gamma}^{\alpha}$ is the plastic shear rate on the α slip which follows a power law relationship shown in Equation 6, $\dot{\gamma}_0$ is the reference shear rate ($\dot{\gamma}_0$=0.001/S in this study), τ_α is the resolved shear stress on α slip, m(=0.05 in this case) is the strain rate sensitive exponent parameter and κ^{α} is the threshold stress of the α slip. h_0 is the initial hardness rate due to dislocation accumulation, κ_s and κ_0 are the saturation strength and the initial strength of the slip, respectively. Details of the formulations are given in the reference [20,21].

Modeling Framework

Magnesium has a hexagonal close-packed (HCP) structure whose deformation modes are different from those of aluminum. Typical deformation modes in magnesium are basal <a>-{0002}<11$\bar{2}$0> slip, prismatic <a>-{10$\bar{1}$0}<11$\bar{2}$0> slip, second pyramidal <c+a>-{11$\bar{2}$2}<11$\bar{2}$3> slip and extension twinning {10$\bar{1}$2}<10$\bar{1}$1>. In this study, a commercial extruded AM30 alloy (mass %, 2.54% Al, 0.40% Mn, Mg in balance) was selected as the HCP experimental material to conduct channel die compression at high temperature 200°C and at strain rate of $10^{-3}S^{-1}$ to strain 30%. At these loading conditions, twinning would not be profuse and, hence, only slip will be the predominant deformation mode. Figure 1 displays the three slip modes used in this study. The hardening parameters of the three slips modes were obtained using material point simulations to fit the experimental stress-strain curve recorded from the channel die compression test. The elasticity parameters used in this study are listed in Table I, while the slip system hardening parameters obtained from the calibration procedure are presented in Table II. Figure 2 compares the predicted and experimental stress-strain curves.

The texture of AM30 was measured by X-ray diffraction method (XRD). The recalculated pole figures were calculated based on the orientation distribution functions (ODFs) which was obtained using the measured six incomplete pole figures {10$\bar{1}$0}, {0002}, {10$\bar{1}$1}, {10$\bar{1}$2}, {11$\bar{2}$0} and {10$\bar{1}$3}. The initial and the channel die compressed texture of AM30 plotted by the texture software MTEX [23] are shown in Figure 4a and 4b, respectively.

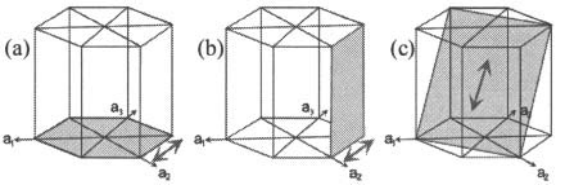

Figure 1: Typical slip deformation modes in magnesium: (a) basal <a>-{0002}<11$\bar{2}$0> slip, (b) prismatic <a>-{10$\bar{1}$0}<11$\bar{2}$0> slip, and (c) second pyramidal <c+a>-{11$\bar{2}$2}<11$\bar{2}$3> slip.

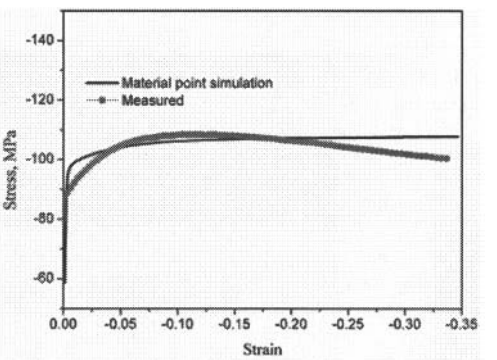

Figure 2: Correlation of the experimentally measured and the material point simulation stress-strain behavior of an AM30 magnesium alloy at 200°C.

Table I. Elasticity parameters for AM30 magnesium alloy.

C_{11}	C_{12}	C_{13}	C_{33}	C_{44}
59.52 GPa	25.6 GPa	21.4 GPa	61.74 GPa	16.47 GPa

Table II. Hardening parameters of the slip modes for AM30 magnesium alloy.

mode	h_0	κ_0	κ_s
Basal <a>	19.6 MPa	18 MPa	20 MPa
Prismatic <a>	37.5 MPa	30 MPa	34 MPa
Pyramidal 2nd <c+a>	18.8 MPa	44 MPa	46 MPa

The commercial finite element software ABAQUS 6.9 and a user subroutine UMAT incorporating the crystal plasticity constitutive theory and the magnesium AM30 materials parameters as listed in Table I and Table II were used to simulate texture evolution and mechanical response. The initial texture used in this CPFEM simulation was measured in the undeformed sample (Figure 4a) and was represented by 343 discrete orientations as shown in Figure 3c. The 3D polycrystal is represented by the 3D Voronoi grains created by the code Neper [24]. The Voronoi 3D grain is evidently more realistic than regular shaped grains used in other studies: brick grains [15,16], rhombic dodecahedron grains and other regular polyhedron grains [13-15,17]. In particular, 3D brick grains are too regular and too uniform in comparison to a realistic grain morphology. The element type used to discretize the Voronoi grains is the second order tetrahedral C3D10 element. As such, one element has four integration points, namely four orientations. There are totally 55092 elements in the Voronoi 3D microstructure. The undeformed polycrystal and the channel die compressed 3D polycrystal up to a strain of 30% are presented in Figures 3a and 3b.

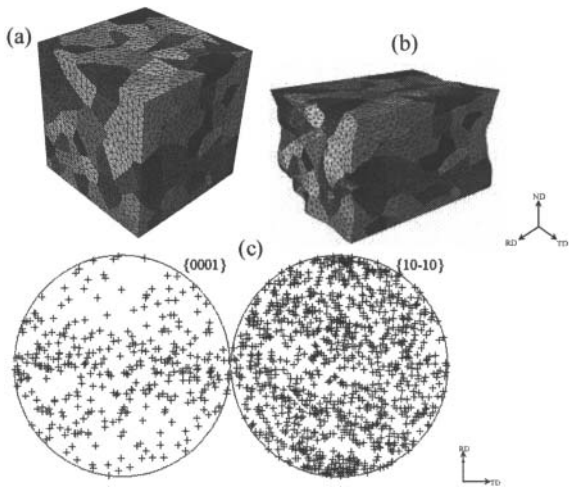

Figure 3: (a) The predeformation 343 3D Voronoi grains and (b) deformed 343 Voronoi grains and (c) the initial 343 discrete orientations representing the initial texture of AM30 magnesium alloy.

Plane strain compression simulations were performed on the 3D polycrystal to strain 30%. Deformation textures were plotted in the {0001} and $\{10\bar{1}0\}$ pole figures using the texture software MTEX [23] with a half scatter width of 7.5 degree.

In order to study intragranular orientation spread in discrete grains, one special orientated grain was selected: grain number123 with a orientation $\{\varphi_1, \Phi, \varphi_2\}=\{190.62, 69.85, -162.48\}$.This grain has 331 elements with a total of 1324 orientations. Note that the analysis of local inhomogeneous deformations in a 3D Voronoi polycrystal has been scarcely treated in the literature [25,26].

In-grain misorientation, namely the orientation spread in one grain indicates the local inhomogeneous orientation distribution and the effect of grain interaction. In addition, the orientation spread of a grain can also characterize the stability property of the grain with a special orientation. The orientation spread $\Delta\theta_i$ in a grain g at various strain levels can be calculated by Equations 9-11. In the specimen coordinate system, one orientation $g_i=\{\varphi_1, \Phi, \varphi_2\}$ can be expressed into the rotation matrix given by Equation 9. There are 12 misorientations Δg_{ij} between two orientations g_i and $\bar{g}$, where g_i is the orientation of an integration point in the grain g and $\bar{g}$ is the mean orientation of all the orientations in the same grain. Δg_{ij} can be calculated by Equation 10 where M_j is the symmetry operator which depends on the symmetry of the HCP crystal system. Usually, the minimum rotation angle $\Delta\theta_i$ defines the misorientation angle or disorientation angle which is expressed as Equation 11.

$$g_i=\begin{pmatrix} \cos\varphi_1\cos\varphi_2-\sin\varphi_1\sin\varphi_2\cos\Phi & \sin\varphi_1\cos\varphi_2+\cos\varphi_1\sin\varphi_2\cos\Phi & \sin\varphi_2\sin\Phi \\ -\cos\varphi_1\sin\varphi_2-\sin\varphi_1\cos\varphi_2\cos\Phi & -\sin\varphi_1\sin\varphi_2+\cos\varphi_1\cos\varphi_2\cos\Phi & \cos\varphi_2\sin\Phi \\ \sin\varphi_1\sin\Phi & -\cos\varphi_1\sin\Phi & \cos\Phi \end{pmatrix} \quad (9)$$

$$\Delta g_{ij}=M_j\cdot g_i\cdot\bar{g}^{-1}=\begin{pmatrix} \Delta g_{11} & \Delta g_{12} & \Delta g_{13} \\ \Delta g_{21} & \Delta g_{22} & \Delta g_{23} \\ \Delta g_{31} & \Delta g_{32} & \Delta g_{33} \end{pmatrix}_{ij} \quad (10)$$

$$\Delta\theta_i=(\arccos(\frac{\Delta g_{11}+\Delta g_{22}+\Delta g_{33}-1}{2})_{ij})\,\min imum \quad (11)$$

Note that $\Delta\theta_i$ is the smallest value among the 12 misoientation angles.

Simulation Results and Discussion

The measured and CPFEM predicted texture are listed in Figure 4. Figure 5 shows the orientation distribution and its spread of grain number 123 as well as its stress and strain localization at strain 30%. The finite element simulation channel die compression stress-strain curve using crystal plasticity model and the measured stress-strain curve are presented in Figure 6.

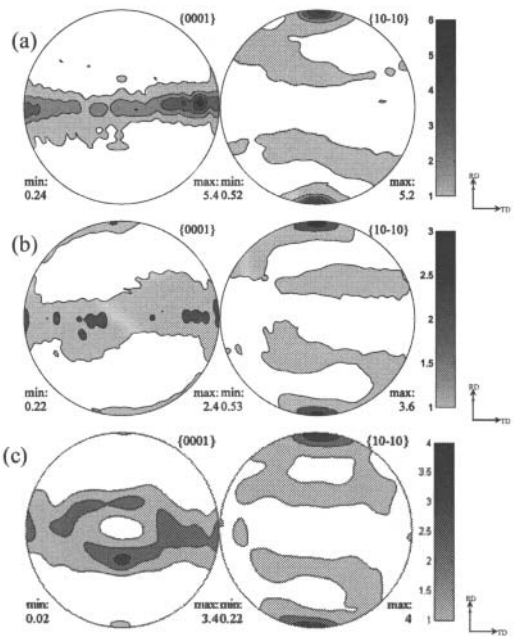

Figure 4: Pole figures for an AM30 magnesium alloy showing (a) the experimental initial texture and (b) the experimental channel die compression at a strain of 30% and (c) the finite element crystal plasticity simulation result at a strain of 30%.

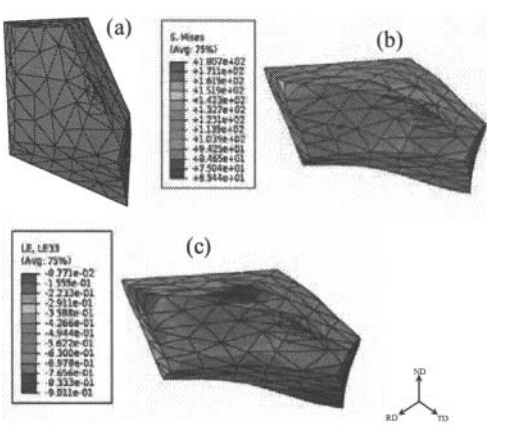

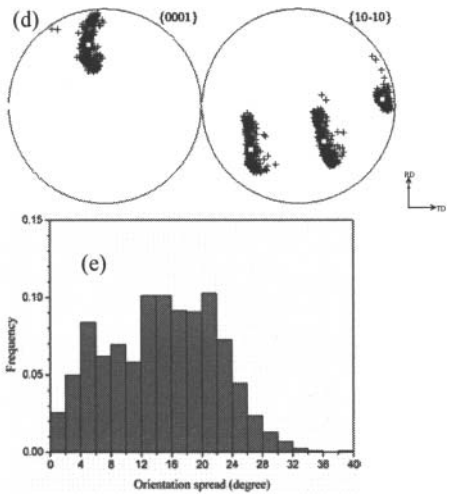

Figure 5: For an AM30 magnesium alloy (a) shows mesh of the initial grain number 123, (b) the local Mises stress and (c) local strain ε_{33} distribution of grain number 123 at a strain of 30%, (d) the orientation distribution of the grain number 123 at a strain of 30%. The cross symbols represent the orientations, the circle symbol represents the initial orientation of grain number 123 and the cube symbol represents the mean orientation among all the orientations, and (e) the orientation spread of the grain number 123 at a strain of 30%.

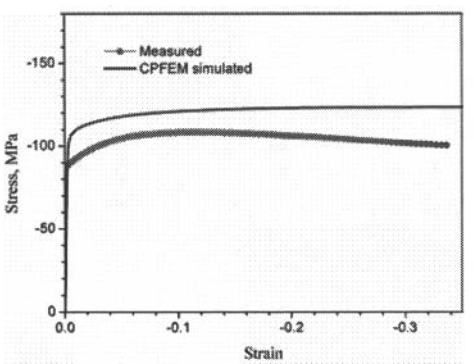

Figure 6: The finite element simulation stress-strain curve based on crystal plasticity model and the experimental stress-strain curve under channel die compression for AM30 magnesium alloy at 200°C.

CPFEM predicted textures of the 3D Voronoi microstructure that are consistent with experimental results as shown in Figure 4b and 4c. As shown by this figure, the measured and the predicted plane strain compression AM30 textures exhibit similar texture configuration. However, there is discrepancy that could stem from the fact that dynamic recrystallization, which typically happens in Mg alloys, is not accounted for in the simulations. Also, the CPFEM simulation stress-strain curve slightly overestimates the stress of the channel die compression. The reason may be due to the effect of grain interaction in the 3D Voronoi microstructure. Figure 5b and 5c present the Mises and ε_{33} strain distribution in grain number 123 at strain 30%. The inhomogeneous deformation of grain number 123 is clearly proved by the observed stress and strain heterogeneous distribution. In addition, as shown in Figure 5d, the grain orientation distribution in grain number 123 displays the different rotation tendency along RD direction. As such, the orientation spread of grain number 123 presents a big scatter with two peaks, as shown in Figure 5e. Accordingly, the effect of grain interaction among this 3D Voronoi polycrystal should play an important role on orientation spread, stress and strain localization and intergranular heterogeneous plasticity.

Conclusions

Plane strain compression simulations of a three dimensional microstructure of HCP magnesium AM30 were performed using an elastic-plastic crystal plasticity model and the finite element method. The mechanical response, global texture evolution and the intergranular heterogeneous plasticity of discrete grain were captured by the 3D Voronoi microstructure channel die compression simulation. Simulation results showed that the effect of grain interaction could play an important role on global texture evolution, the orientation spread and the local heterogeneity deformation of one grain.

Acknowledgements

The authors are grateful to the financial support from the Department of Energy, Contract No. DE-FC-26-06NT42755, and the Center for Advanced Vehicular Systems (CAVS) at Mississippi State University.

References

1. D. Raabe, "Yield surface simulation for partially recrystallized aluminum polycrystals on the basis of spatially discrete data," *Computational Materials Science,* 19 (2000), 13-26.
2. A. Fjeldly and H.J. Roven, "Observations and calculations on mechanical anisotropy and plastic flow of an AlZnMg extrusion," *Acta Materialia,* 44 (1996), 3497-3504.
3. G. Sachs, "Zur ableitung einer fleissbedingun," *Zeichschrift Verein Deutscher Ingenieur,* 72 (1928), 734-736.
4. GI. Taylor, "Plastic strain in metals," *Journal of the Institute of Metals,* 62 (1938), 307-324.
5. D. Raabe, Z. Zhao, and W. Mao, "On the dependence of in-grain subdivision and deformation texture of aluminum on grain interaction," *Acta Materialia,* 50 (2002), 4379-4394.
6. P. Van Houtte et al., "Deformation texture prediction: From the Taylor model to the advanced Lamel model," *International Journal of Plasticity,* 21 (2005), 589-624.
7. U.F. Kocks and H. Chandra, "Slip geometry in partially constrained deformation," *Acta Metallurgica,* 30 (1982), 695-709.
8. W. Mao and Y. Yu, "Effect of elastic reaction stress on plastic behaviors of grains in polycrystalline aggregate during tensile deformation,"*Materials Science and Engineering,* A367 (2004) 277-281.
9. R.A. Lebensohn and C.N. Tomé, "A self-consistent anisotropic approach for the simulation of plastic deformation and texture development of polycrystals: Application to zirconium alloys," *Acta Materialia,* 41 (1993), 2611-2644.
10. D. Peirce, R.J. Asaro, and A. Needleman, "Material rate dependence and localized deformation in crystalline solids," *Acta Metallurgica,* 31 (1983), 1951-1976.
11. D. Peirce, R.J. Asaro, and A. Needleman, "Analysis of nonuniform and localized deformation in ductile single crystals," *Acta Metallurgica,* 30 (1982), 1087-1119.
12. A. Alankar, Ioannis N. Mastorakos, and D.P. Field, "A

dislocation-density-based 3D crystal plasticity model for pure aluminum," *Acta Materialia,* 57 (2009), 5936-5946.
13. E.B. Marin and P.R. Dawson, "Elastoplastic finite element analyses of metal deformations using polycrystal constitutive models,"*Computer Methods in Applied Mechanics and Engineering,* 165 (1998), 23-41.
14. F. Roters et al., "Overview of constitutive laws, kinematics, homogenization and multiscale methods in crystal plasticity finite-element modeling: Theory, experiments, applications,"*Acta Materialia*, 58 (2010), 1152-1211.
15. Z. Zhao et al., "Influence of in-grain mesh resolution on the prediction of deformation textures in fcc polycrystals by crystal plasticity FEM," *Acta Materialia,* 55 (2007), 2361-2373.
16. G.B. Sarma and P.R. Dawson, "Effects of interactions among crystals on the inhomogeneous deformations of polycrystals ," *Acta Materialia,* 44 (1996), 1937-1953.
17. D.P. Mika and P.R. Dawson, "Effects of grain interaction on deformation in polycrystals ," *Materials Science and Engineering,* A257 (1998), 62-76.
18. P.R. Dawson, D.P. Mika, and N.R. Barton, "Finite element modeling of lattice misorientations in aluminum polycrystals," *Scripta Materialia,* 47 (2002), 713-717.
19. D.P. Mika and P.R. Dawson, "Polycrystal plasticity modeling of intracrystalline boundary textures," *Acta Materialia,* 47 (1999), 1355-1369.
20. E.B. Marin, "On the formulation of a crystal plasticity model" (Report SAND2006-4170, Sandia National Laboratories, CA, 2006).
21. S. Groh et al., "Multiscale modeling of the plasticity in an aluminum single crystal,"*International Journal of Plasticity,* 25(2009), 1456-1473.
22. E.B. Marin and P.R. Dawson, "On modeling the elasto-visoplastic response of metals using polycrystal plasticity," *Computer Methods in Applied Mechanics and Engineering,* 165 (1998), 1-21.
23. R. Hielscher and H. Schaeben, "A novel pole figure inversion method: specification of the MTEX algorithm," *Journal of Applied Crystallography,* 41 (2008), 1024-1037.
24. http://neper.sourceforge.net
25. M. Blicharski, R. Becker, and H. Hu, "Deformation texture of channel-die deformed aluminum bicrystals with *S* orientations," *Acta Metallurigica et Materialia,* 41 (1993), 2007-2016.
26. Y.L. Liu, H. Hu, N. Hansen, "Deformation and recrystallization of a channel die compressed aluminium bicrystal with (112)[111]/(123)[412] orientation," *Acta Metallurigica et Materialia,* 43 (1995), 2395-2405.